Multisource Earth Observation Data for Land-Cover Classification Using Random Forest

Zhigang Xu, Jike Chen, Junshi Xia, *Member, IEEE*, Peijun Du, *Senior Member, IEEE*, Hongrui Zheng, and Le Gan

***Abstract*— In this letter, multisource earth observation (EO) data sets, including multitemporal Landsat-8, digital surface model, and spatial information, were integrated for land-cover classification by random forest (RF) and support vector machines (SVMs). We demonstrated in this letter that both RF and SVM are useful tools for classification of land cover in the local climate zones featured with highly heterogeneous landscape. Classification of land cover by RF was with an overall accuracy (OA) of 86.2%, while the OA was 85.5% for SVM. However, we found that RF was more stable than SVM for multisource EO data in classifying land cover without normalizing different feature data sets. Experiments showed that the thermal features were more important than temporal and spatial ones in discriminating impervious objects, while the temporal and spatial features were generally better than thermal ones in separating the distinct vegetation categories. Another finding was that our experiments indicated that spectral features were the most important in classification of land cover, followed by temporal, thermal, and spatial features, respectively. As to the spectral features, red channels were the most important, followed by short-wave infrared, near-infrared, and green channels. Thus, it could be concluded that the combination of spectral, thermal, spatial, and temporal information would be an optimal approach to increase the OA of land-cover classification in the zones featured with highly heterogeneous landscape.**

***Index Terms*— Digital surface model (DSM), land cover, local climate zones (LCZs), random forest (RF), thermal infrared sensor (TIRS).**

I. Introduction

NOWADAYS, worldwide urbanization is unprecedentedly in process. Rapid urbanization has resulted in that much natural land cover being converted to artificial land cover. The structure and fabric of the land surface have also simultaneously changed, triggering environmental and ecological risks. Finely classifying the land cover according to the structure, cover, and fabric of the urban area has become critical for climate and environment research on urban areas [1].

In the recent decades, earth observation (EO) has been proven to be the most useful and efficient approach for land-cover classification [2]–[7] because it can acquire large-scale land-cover information quickly and repeatedly. Some researchers achieved better classification results by integrating useful information, such as spectral, spatial, thermal, and temporal information based on multisource EO data.

Spatial features can provide the topographic and structure information of the land surface to improve the classification performance. Bechtel and Daneke [8] showed that the spatial structure features [i.e., morphological attribute profiles (MAPs)] can be exploited to complement the spectral features to improve the mapping accuracy in urban areas. Wang *et al.* [9] integrated spatial topographical feature elevation and slope into multispectral features to produce a finer land-cover classification map. Temporal information was also added to the classification procedure to reduce the misclassifications of different vegetation types, which raises land-cover classification accuracy [10]. Some classes of land cover have different thermal radiance characteristics. Therefore, thermal features were combined with multitemporal spectral bands to increase the discrimination of bare soil and poplar grove categories [11].

Although many studies on the multisource EO data fusion indicated its great ability and potential for land-cover classification, the strategy of combining spectral, spatial, temporal, and thermal information is an open question. Meanwhile, selecting a good classification method and assessing the importance of different features are the two key components for the classification process. In this letter, an ensemble learning technique, called random forest (RF), is chosen as the classifier because it can provide a great classification performance in an effective manner and assess the importance of the input features. RF has been successfully applied to discriminate tree species [12], classify land cover [11] and urban scenes [13], generate wetland maps [14], and map forest [15] fusing multisource EO data.

All aforementioned studies indicated that RF can deal with multisource high-dimensional data. These data include different kinds of features with different value ranges. However, a few studies focused on evaluating the feature importance of the spectral, temporal, thermal, and spatial information, especially for digital surface model (DSM), MAPs derived from DSM, and information in land-cover classification tasks, and assessing the stability of RF rather than focusing on other

Manuscript received December 20, 2017; accepted January 13, 2018. Date of publication March 6, 2018; date of current version April 20, 2018. This work was supported in part by the National Natural Science Foundation of China under Grant 41631176, in part by the Fujian Province Natural Science Foundation of China under Grant 2017J01662, and in part by the Fujian Province Outstanding Youth Scientific Research Personnel Training Program Foundation of China. *(Corresponding author: Peijun Du.)*

Z. Xu is with the Key Laboratory for Satellite Mapping Technology and Applications, National Administration of Surveying, Mapping and Geoinformation of China, Nanjing University, Nanjing 210023, China, and also with the School of Resource Engineering, Longyan University, Longyan 364012, China (e-mail: xzg_xzg1982@163.com).

J. Chen, P. Du, H. Zheng, and L. Gan are with the Key Laboratory for Satellite Mapping Technology and Applications, National Administration of Surveying, Mapping and Geoinformation of China, and also with the Jiangsu Provincial Key Laboratory of Geographic Information Science and Technology, Nanjing University, Nanjing 210023, China (e-mail: cjike12@126.com; dupjrs@gmail.com; myzhenghr@126.com; lelegan@126.com).

J. Xia is with the Research Center for Advanced Science and Technology, The University of Tokyo, Tokyo 153-8904, Japan (e-mail: xiajunshi@gmail.com).

Color versions of one or more of the figures in this letter are available online at http://ieeexplore.ieee.org.

Digital Object Identifier 10.1109/LGRS.2018.2806223

1545-598X © 2018 IEEE. Personal use is permitted, but republication/redistribution requires IEEE permission.
See http://www.ieee.org/publications_standards/publications/rights/index.html for more information.

Authorized licensed use limited to: Nanjing University. Downloaded on January 15,2024 at 11:13:15 UTC from IEEE Xplore. Restrictions apply.

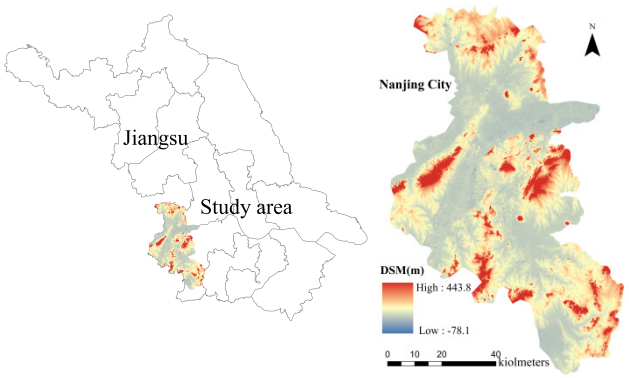

Fig. 1. Location of the study area.

state-of-the-art classifiers for feature value normalization using the multisource EO data.

The objective of this letter is to present a classification scheme combining spectral, spatial, thermal, and temporal feature sets for vast areas with a complex landscape using RF and compare it with well-known support vector machines (SVMs). This letter focuses on the following questions.

1) Can a large highly heterogeneous landscape in local climate zones (LCZs) be well classified by fusing four feature sets using RF?
2) Is RF more stable than SVM?
3) What is the importance of each feature for the global and per-class accuracies of the land cover?

II. Data and Methods

A. Study Areas and Classification Scheme

Nanjing city (excluding the Gaochun District), which is the capital of Jiangsu province, China, was selected as the study area (Fig. 1). The study area measured 6069.52 km^2, and had an altitude ranging approximately from 1.4 to 360.6 m and an average elevation of 25 m. The main land-cover types comprise farmland, woodland, impervious surface, water, bare soil, etc.

The land cover was divided into eight classes based on the structure, cover, and fabric of the land surface in the LCZ [1]: high-rise building (HB), mid-rise building, low-rise building, other impervious, woodland, low plant (LP), bare soil, and water.

B. Multisource Earth Observation Data and Features

Two temporal Landsat-8 images were acquired on September 2, 2015 (summer) and March 12, 2016 (spring). For the multispectral bands, the top of the atmosphere reflectance products acquired by radiometric calibration using ENVI5.3 software was sufficient for the classification purpose [16]. The thermal bands were converted into brightness temperatures and resampled to 30 m.

The DSM data had better than 15-m planar accuracy and 5-m vertical accuracy derived from the resource satellite three (ZY-3) images in 2015 using geometric precision correction. The DSM data were registered to Landsat-8 images under less than one-half pixel root-mean-square error and resampled to 30 m. In addition to the DSM, MAPs also provided extra spatial information to improve the classification accuracy [17].

TABLE I
Feature Sets and the Number of Features n per Set

Feature set	Name of variables	N
Spectral feature (F1)	C1, B1, G1, R1, N1, S11, S12	7
Thermal feature (F2)	T11, T12	2
Spatial feature (F3)	D, E1, E2	3
Temporal feature (F4)	C1, B1, G1, R1, N1, S11, S12, T11, T12	18

Note: C1, B1, G1, R1, N1, S11, S12, T11, T12, C2, B2, G2, R2, N2, S21, S22, T21, and T22: coastal (C); blue (B); green (G); red (R); near-infrared (NIR); short-wave infrared 1 (SWIR1); SWIR2; thermal infrared sensor 1 (TIRS1); TIRS2 bands of Landsat-8 of spring and summer; and D, E1, E2: DSM and PC 1 and PC 2 of MAPs.

The attributes comprised purely geometric (area) and textural (standard deviation) to achieve beneficial spatial information. The rational threshold values for each attribute were used by an automatic scheme [17]. Furthermore, the spatial features derived from MAPs were transformed by a principal component analysis for dimensionality reduction. Furthermore, the first two principal components (i.e., PC1 and PC2) retaining more than 99% variance were used to classify the land cover. The DSM data were complementary: the multitemporal RF images provided spectral, thermal, and temporal information, whereas the DSM and MAPs provided spatial topography and structure information.

Table I shows the four different feature sets used in this letter.

C. RF-Based Classification Schemes

RF is an ensemble classification method that evolves from the bagging method proposed by Breiman [18]. RF uses many independent individual classification and regression trees (CARTs) as the base classifier $\{h(X, \theta_k), k = 1, \ldots\}$, where h stands for the RF classifier, x is the input vector, and $\{\theta_k\}$ are the independent identically distributed random vectors, from which all the CARTs are generated. For classification, each tree casted a unit vote for the most popular class at each input instance. The final label was determined by a majority vote of the trees. Note that the RF can measure the feature importance processed out-of-bag data by means of the permutation importance measure [18].

We designed the following six scenarios to assess the stability of RF and examine the effect of different feature sets on the classification accuracy: 1) scenario 1: F1; 2) scenario 2: F1 and F2; 3) scenario 3: F1 and F3; 4) scenario 4: F4; 5) scenario 5: F1, F2, and F3; and 6) scenario 6: F3 and F4.

D. Reference Data

The ground reference data were collected by utilizing the visual interpretation of high-spatial-resolution images from Google Earth. Subsequently, 20% of the reference samples were randomly selected as a training set, and the remaining 80% was used as the testing set to evaluate the classification accuracy (Table II). The accuracy measures employed in the process of accuracy assessment contained overall accuracy (OA), user's accuracy (UA), and producer's accuracy (PA) [19].

III. Results and Discussion

In the experiments, RF is first utilized to execute the classification process according to the scheme of six scenarios.

Authorized licensed use limited to: Nanjing University. Downloaded on January 15,2024 at 11:13:15 UTC from IEEE Xplore. Restrictions apply.

TABLE II
GROUND REFERENCE DATA FOR EACH OF THE CLASSES

Class	Description	Train	Test
Low-plant (LP)	Grassland and farmland	5269	21075
High-rise building (HB)	Above 10 stories buildings	840	3361
Low-rise building (LB)	1–3 stories buildings	2600	10400
Mid-rise building (MB)	3–9 stories buildings	1061	4244
Other-impervious (OI)	Bare rock and paved cover	830	3318
Bare-soil (BS)	Bare soil and bare sand	243	974
Water (WT)	All kinds of water bodies	878	3511
Woodland (WL)	Forest and bush	2391	9564
	Total samples	14112	56447

TABLE III
COMPARISON OF OA (%) BEFORE AND AFTER NORMALIZATION FOR RF AND SVM

Scenarios	RF		SVM	
	BF	AF	BF	AF
Scenario 1	77.9 ± 0.11	77.7 ± 0.07	80.4 ± 0.13	80.4 ± 0.11
Scenario 2	81.4 ± 0.16	81.4 ± 0.11	83.5 ± 0.11	84.1 ± 0.05
Scenario 3	81.0 ± 0.09	80.9 ± 0.14	**75.7 ± 0.21**	**80.4 ± 0.11**
Scenario 4	81.9 ± 0.10	81.8 ± 0.06	**84.1 ± 0.09**	**84.1 ± 0.31**
Scenario 5	83.6 ± 0.09	83.7 ± 0.11	78.4 ± 0.17	**82.7 ± 0.19**
Scenario 6	**86.4 ± 0.10**	86.2 ± 0.06	82.2 ± 0.09	**85.5 ± 0.16**

Note: BF is OA using the original values of every feature. AF is OA using the normalized values of every feature.

Besides, another widely used classifier SVM is also employed for a comparison with RF. For the RF method, two important parameters should be set: the randomly selected features (m) and number of trees (k). Default parameters are set to $m = \sqrt{n}$, where n is the number of the inputted features [12], and the number of trees k is fixed to be 200. As for SVM, the radial basis function is chosen as the kernel function and its optimal parameters (C and γ) are obtained by grid-search method.

A. RF and SVM Stability Comparison

Table III displays the OA of the RF and the SVM averaged on ten random trials from the training and test samples with 95% confidence intervals for six scenarios.

The first analysis of OA showed a comparison of the RF with the SVM for six scenarios. There is little change in OA values of RF, and of SVM fusing similar feature data sets before and after normalization, but OA values significantly increase fusing different feature data sets which are normalized for SVM.

From Table III, both classifiers showed their ability to tackle the classification problem of the multisource EO data with an OA of 86.2% for the RF and 85.5% for the SVM. The normalization process has little influence on the classification results using RF classifier. However, it plays an important role for SVM classifier. Good performance is also achieved by normalizing features for SVM.

B. Comparison of the Classification Results With Different Feature Fusions

In this letter, we investigated the effect of the spectral feature set fusing the thermal, spatial, and temporal feature sets for the classification of a large heterogeneous landscape by the RF. Table IV shows the result. Several findings are revealed as follows.

1) Scenario 1 produced the lowest OA 77.9%. The PA and the UA of HB, mid-rise building, and other impervious are only 37.8%, 38.5%, 24.3%, 45%, 44.7%, and 38.6%. It effectively failed to discriminate different impervious classes.
2) The classification accuracy in scenario 2 increased compared with that in scenario 1. The best OA reached an 81.4% and 4.4% point increment over scenario l. As regards PA and UA, the HB, low-rise building, mid-rise building, and other impervious achieved 53%, 2%, 23%, 78%, 41%, 7%, 17%, and 53% increments. The performance of the impervious objects was remarkably improved because the thermal feature set significantly increased the interclass discrimination. Meanwhile, the separability between the bare soil and the LP was enlarged to improve the accuracy of the bare soil, which resulted in the accuracy increment of 3.4% and 10.2% points.
3) Scenario 3 integrated the spatial features into multispectral and gained results comparable with those in scenario 2. It also greatly enhanced the performance of HB, low-rise building, mid-rise building, other impervious, and bare soil. Nevertheless, it caused an accuracy of HB and other impervious lower than those in scenario 2.
4) Scenario 4, in which two temporal sets of multispectral feature sets were fused, improved all kinds of accuracies for each class, especially for bare soil, LP, and woodland. It also obtained a better OA than those of scenarios 1 and 2.
5) Scenario 5 combined thermal information, spatial information, and spectral information. The accuracies further increased compared to those of scenarios 2 and 3. The thermal and spatial information were mutually complementary for improving the classification performance.
6) Temporal information was added in scenario 5, while the highest OA of 86.4% was achieved in scenario 6. The per-class accuracy of HB, other impervious, and bare soil increased by 3%, 16%, and 19% points for PA and 7%, 10%, and 6% points for UA when compared with those of scenario 5. The main reasons were that the multitemporal operational land imager bands can provide phenological information to separate the classes of bare soil, LP, and woodland. Fig. 2 presents the classification maps. We can draw that the fusion of spectral, thermal, spatial, and temporal evidently promoted the classification results to efficiently and finely classify the large heterogeneous landscape.

C. Feature Importance for the Global and Class Accuracies

A uniform training set (1200 samples per class) was selected to evaluate the feature importance for global and each class and avoid the biases caused by some classes of a less number of samples in scenario 5 [13].

Fig. 3 presents the feature importance for the calculated global accuracy. The most relevant features for the global were R2, S22, S21, N2, G1, and R1, followed by T11, T22, G2, T21, N1, S12, B2, S11, C2, B1, C1, and T12. The relevance of the spatial features (i.e., D, E1, and E2) was the least. The main possible reasons for this are listed as follows.

1) Coarser spatial resolution and lower noise–signal ratio of the thermal infrared sensor (TIRS) bands.

Authorized licensed use limited to: Nanjing University. Downloaded on January 15,2024 at 11:13:15 UTC from IEEE Xplore. Restrictions apply.

TABLE IV
OA (%), PER-CLASS PA (%), AND UA (%) OF FIVE SCENARIOS

scenarios	LP		HB		LB		MB		OI		BS		WT		WL		OA
	PA	UA	PA	UA	PA	UA	PA	UA	PA	UA	PA	UA	PA	UA	PA	UA	
Scenario1	93.2	86.0	37.8	45.0	78.8	71.0	38.5	44.7	24.3	38.6	60.1	75.0	90.7	92.6	90.6	93.7	77.9±0.11
Scenario2	93.6	86.6	57.8	63.3	80.1	75.7	47.3	52.4	43.2	59.0	62.2	82.7	91.0	92.9	90.9	94.6	81.4±0.16
Scenario3	94.6	87.3	46.9	62.6	81.0	72.2	48.6	53.3	36.3	49.5	65.6	82.2	90.3	94.3	90.8	95.5	81.0±0.09
Scenario4	95.1	89.5	45.4	53.2	83.0	73.4	43.4	52.4	43.2	56.2	73.2	86.6	93.2	94.4	91.3	94.9	81.9±0.10
Scenario5	95.1	87.5	61.3	69.3	83.1	76.2	55.3	62.7	46.5	67.7	65.8	85.7	91.2	93.7	91.1	96.2	83.6±0.09
Scenario6	**96.4**	**90.1**	**69.3**	**74.1**	**86.8**	**80.0**	**58.8**	**65.8**	**53.7**	**74.5**	**78.1**	**91.2**	**93.4**	**95.5**	**91.7**	**97.1**	**86.4±0.10**

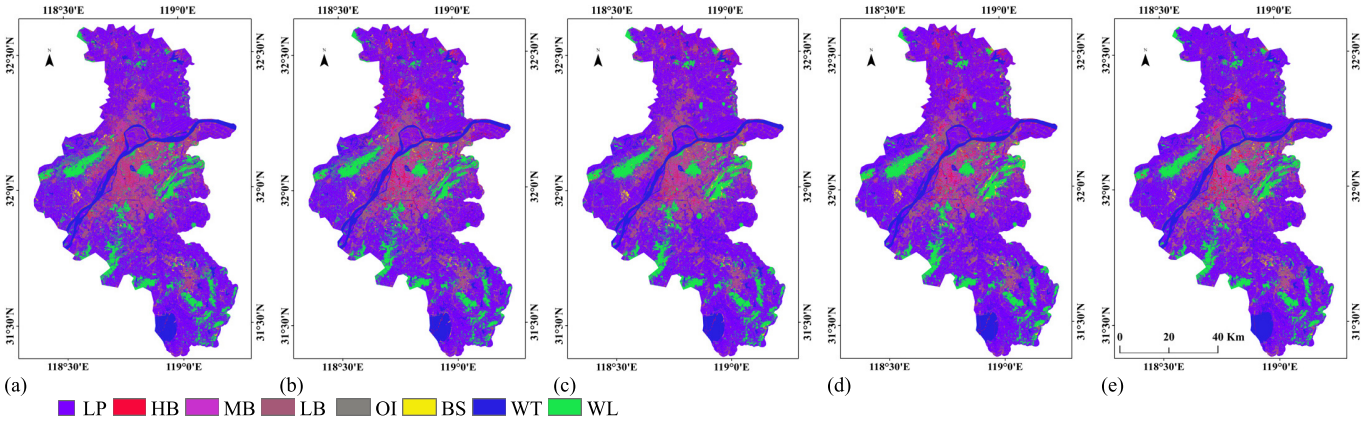

Fig. 2. Classification maps obtained with RF classifier considering (a) scenario 1, OA = 77.9%, (b) scenario 2, OA = 81.4%, (c) scenario 3, $OA = 81\%$, (d) scenario 5, OA = 83.6%, and (e) scenario 6, OA = 86.4%.

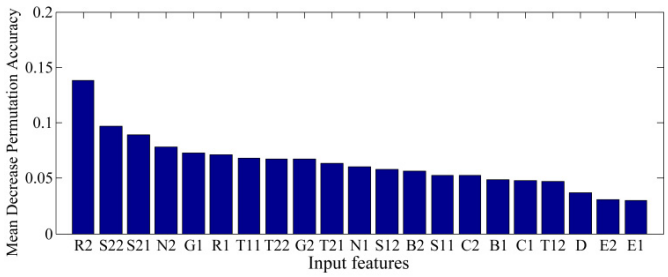

Fig. 3. Feature importance by mean decrease permutation accuracy.

2) Coarser topography and morphology information provided by the spatial features, and the reflectance in the study area was high for the bare soil (lateritic soil) [13] and inversely low for the impervious in the R channel [20]. The LP and the woodland with vegetation information had a high reflectance in the NIR and G channels, respectively, which discriminated them from the other classes. Near infrared (NIR) and short-wave infrared (SWIR) were almost absorbed for water. All the above mentioned led to a greater importance of the four spectral features (i.e., R, SWIR, NIR, and G). The rest of features will be explained for each class.

Fig. 4 shows the importance of the features of individual class. The most important features for the LP were the NIR bands of double temporal and the B and R bands of summer. This class was mixed with vegetation and bare soil. The bare-soil component made it possess a high reflectance in the B and R bands, which were beneficial for separation from the woodland. The reflectance of the vegetation component was strong in the NIR bands, allowing the recognition of the LP from the bare soil.

Regarding HB, in addition to the four TIRS bands of two temporal sets, the third spatial feature was very discriminating. The radiance and structure information of the HB class were different from those of the other low impervious objects. The multispectral bands in this class did not seem to be very important because they were not suitable for discriminating objects with a distinct height.

Low-rise building and other impervious showed more importance in the two SWIR bands of summer and the two TIRS bands of spring. As expected, the spectral signatures were different between the impervious surface and the bare soil in SWIR [20] and among the impervious objects with different heights in TIRS [1], which explained the relativity of a couple of features for the two classes.

Regarding the mid-rise building, the feature importance was more scattering among the spectral, thermal, spatial, and temporal sets, which made the separation more difficult (Table IV). Three spatial features seemed to be more relevant than some multispectral bands (i.e., G, R, and SWIR bands of spring) because the spatial features can provide spatial structure information to discriminate different objects with distinct heights.

The bare soil in the study area was substantially composed of lateritic soil with high reflectance in the two R bands of spring and summer, resulting in a great importance of this band. As for the G and two SWIR bands of summer, the bare soil usually covered by less grass in summer was different from the impervious objects in the G band and LP and impervious objects in the SWIR bands, which interpreted the relative importance of the G and SWIR bands, respectively.

For water, two NIR and four SWIR bands of double temporal showed a high level of importance. Indeed, the relatively low reflectance was specific to water. Conversely, the spatial

Authorized licensed use limited to: Nanjing University. Downloaded on January 15,2024 at 11:13:15 UTC from IEEE Xplore. Restrictions apply.

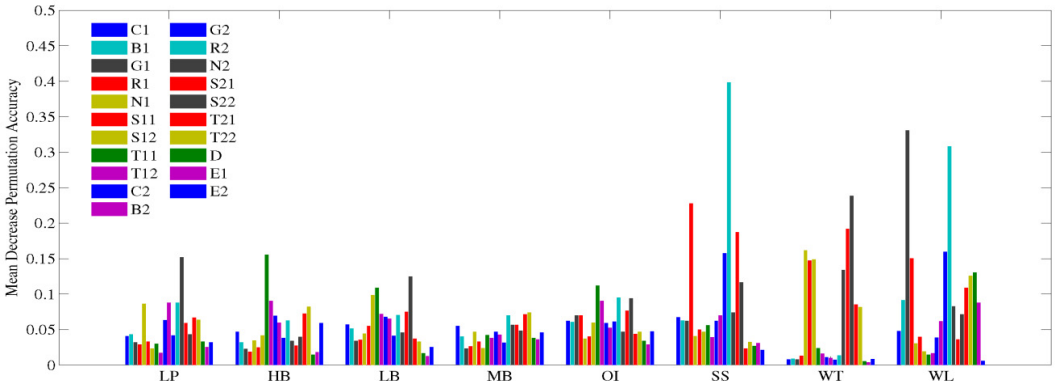

Fig. 4. Feature importance per class by mean decrease permutation accuracy.

features were least important because water had no clear structure information.

The woodland showed greater importance in the G and R bands of the two seasons when compared to the other multispectral bands. In general, dense vegetation scenes with high reflectance in G and strong absorption in R were different from the other classes. In addition, two TIRS bands of summer and two spatial features seemed to be more relevant for this category as the woodland separated from the LP in the information of topographical, structural, and thermal radiance.

IV. Conclusion

This letter aims to assess the performance of the RF classifier for the land-cover classification of a heterogeneous area (i.e., Nanjing city) and evaluate the feature importance for global and per class. Fusing spectral, thermal, spatial, and temporal features, the RF performed well in the scheme of classifications with eight classes without normalizing for different features, and was more stable than the SVM with respect to the multisource EO data. Moreover, the RF classifier provided the permutation accuracy criteria for evaluating the importance of each feature for the global accuracy and individual class. In summary, the spectral feature set was more important than the thermal feature set and the spatial feature set in the classification process. The most relevant features in the spectral feature set were the R, SWIR, NIR, and G channels. The spectral information in the spring Landsat image was more conducive to the classification performances than that in the summer Landsat image. However, the thermal features were vitally important for some specific classes, such as HBs, low-rise buildings, mid-rise buildings, and other impervious, in which temperature was a critical factor. The spatial feature set greatly influenced the woodland, LP, and mid-rise building classes.

References

[1] I. D. Stewart and T. R. Oke, "Local climate zones for urban temperature studies," *Bull. Amer. Meteorol. Soc.*, vol. 93, no. 12, pp. 1879–1900, Dec. 2012.

[2] P. Gong *et al.*, "Finer resolution observation and monitoring of global land cover: First mapping results with Landsat TM and ETM+data," *Int. J. Remote Sens.*, vol. 34, no. 7, pp. 2607–2654, Dec. 2013.

[3] Q. Wang, J. Lin, and Y. Yuan, "Salient band selection for hyperspectral image classification via manifold ranking," *IEEE Trans. Neural Netw. Learn. Syst.*, vol. 27, no. 6, pp. 1279–1288, Jun. 2016.

[4] Q. Wang, G. Zhu, and Y. Yuan, "Multi-spectral dataset and its application in saliency detection," *Comput. Vis. Image Understand.*, vol. 117, no. 12, pp. 1748–1754, Dec. 2013.

[5] Q. Wang, J. Fang, and Y. Yuan, "Multi-cue based tracking," *Neurocomputing*, vol. 131, pp. 227–236, May 2014.

[6] X. Peng, J. Lu, Z. Yi, and R. Yan, "Automatic subspace learning via principal coefficients embedding," *IEEE Trans. Cybern.*, vol. 47, no. 11, pp. 3583–3596, Nov. 2017.

[7] X. Peng, C. Lu, Z. Yi, and H. Tang, "Connections between nuclear-norm and Frobenius-norm-based representations," *IEEE Trans. Neural Netw. Learn. Syst.*, vol. 29, no. 1, pp. 218–224, Jan. 2018.

[8] B. Bechtel and C. Daneke, "Classification of local climate zones based on multiple earth observation data," *IEEE J. Sel. Topics Appl. Earth Observ. Remote Sens.*, vol. 5, no. 4, pp. 1191–1202, Aug. 2012.

[9] Y.-C. Wang, C.-C. Feng, and H. V. Duc, "Integrating multi-sensor remote sensing data for land use/cover mapping in a tropical mountainous area in northern Thailand," *J. Geophys. Res.*, vol. 50, no. 3, pp. 320–331, Aug. 2012.

[10] B. Chen, B. Huang, and B. Xu, "Multi-source remotely sensed data fusion for improving land cover classification," *ISPRS J. Photogramm. Remote Sens.*, vol. 124, pp. 27–39, Feb. 2017.

[11] V. F. Rodríguez-Galiano, B. Ghimire, E. Pardo-Igúquiza, M. Chica-Olmo, and R. G. Congalton, "Incorporating the downscaled Landsat TM thermal band in land-cover classification using random forest," *Photogramm. Eng. Remote Sens.*, vol. 78, no. 2, pp. 129–137, Feb. 2012.

[12] L. Naidoo, M. A. Cho, R. Mathieu, and G. Asner, "Classification of savanna tree species, in the Greater Kruger National Park region, by integrating hyperspectral and LiDAR data in a Random Forest data mining environment," *ISPRS J. Photogramm. Remote Sens.*, vol. 69, pp. 167–179, Apr. 2012.

[13] L. Guo, N. Chehata, C. Mallet, and S. Boukir, "Relevance of airborne lidar and multispectral image data for urban scene classification using Random Forests," *ISPRS J. Photogramm. Remote Sens.*, vol. 66, no. 1, pp. 56–66, Jan. 2011.

[14] J. M. Corcoran, J. F. Knight, and A. L. Gallant, "Influence of multi-source and multi-temporal remotely sensed and ancillary data on the accuracy of random forest classification of wetlands in Northern Minnesota," *Remote Sens.*, vol. 5, no. 7, pp. 3212–3238, Jul. 2013.

[15] A. Mellor, A. Haywood, S. Jones, and P. Wilkes, "Forest classification using random forests with multisource remote sensing and ancillary GIS data," presented at the 16th Austral. Remote Sens. Photogramm. Conf., Melbourne, VIC, Australia, Aug. 2012.

[16] C. Song, C. E. Woodcock, K. C. Seto, M. P. Lenney, and S. A. Macomber, "Classification and change detection using Landsat TM data: When and how to correct atmospheric effects?" *Remote Sens. Environ.*, vol. 75, no. 2, pp. 230–244, Feb. 2001.

[17] P. Ghamisi, J. N. A. Benediktsson, and J. R. Sveinsson, "Automatic spectral–spatial classification framework based on attribute profiles and supervised feature extraction," *IEEE Trans. Geosci. Remote Sens.*, vol. 52, no. 9, pp. 5771–5782, Sep. 2014.

[18] L. Breiman, "Random forests," *Mach. Learn.*, vol. 45, no. 1, pp. 5–32, Apr. 2001.

[19] R. G. Congalton, "A review of assessing the accuracy of classifications of remotely sensed data," *Remote Sens. Environ.*, vol. 37, no. 1, pp. 35–46, Dec. 1991.

[20] H. Xu, "Analysis of impervious surface and its impact on urban heat environment using the normalized difference impervious surface index (NDISI)," *Photogramm. Eng. Remote Sens.*, vol. 76, no. 5, pp. 557–565, May 2010.

Authorized licensed use limited to: Nanjing University. Downloaded on January 15,2024 at 11:13:15 UTC from IEEE Xplore. Restrictions apply.